Supercurrent as a probe for topological superconductivity in magnetic adatom chains

Narayan Mohanta,[1,2] Arno P. Kampf,[1] and Thilo Kopp[2]
[1]*Center for Electronic Correlations and Magnetism, Theoretical Physics III, Institute of Physics, University of Augsburg, 86135 Augsburg, Germany*
[2]*Center for Electronic Correlations and Magnetism, Experimental Physics VI, Institute of Physics, University of Augsburg, 86135 Augsburg, Germany*

(Received 6 October 2017; published 11 June 2018)

A magnetic adatom chain, proximity coupled to a conventional superconductor with spin-orbit coupling, exhibits locally an odd-parity, spin-triplet pairing amplitude. We show that the singlet-triplet junction, thus formed, leads to a net spin accumulation in the near vicinity of the chain. The accumulated spins are polarized along the direction of the local **d** vector for triplet pairing and generate an enhanced persistent current flowing around the chain. The spin polarization and the "supercurrent" reverse their directions beyond a critical exchange coupling strength at which the singlet superconducting order changes its sign on the chain. The current is strongly enhanced in the topological superconducting regime where Majorana bound states appear at the chain ends. The current and the spin profile offer alternative routes to characterize the topological superconducting state in adatom chains and islands.

DOI: 10.1103/PhysRevB.97.214507

I. INTRODUCTION

Artificial lattices of magnetic adatoms, such as Fe, Cr, or Gd, deposited on a spin-orbit coupled conventional superconductor, provide a versatile platform to realize Majorana bound states (MBS), locally accessible via scanning tunneling microscopy (STM) [1–9]. Unlike the heterostructure-based schemes [10–13], these adatom lattices can exhibit topological superconductivity (TSC) even in the absence of spin-orbit coupling (SOC) when the adatom moments within a chain form a real-space helix [14–16]. The adatoms act as magnetic impurities for the host superconductor and give rise to Yu-Shiba-Rusinov (YSR) states which hybridize to form a band dispersing within the energy gap of the superconductor [17–20]. In suitable parameter regimes, SOC induces chiral TSC in the YSR impurity band [16,21–37]. An adatom chain, therefore, mimics the physics of the one-dimensional Kitaev model [38] which contains isolated MBS at the ends of the chain. Experimental signatures for the possible existence of MBS on magnetic adatom chains were reported in recent STM experiments [4–8].

The broken inversion symmetry at an interface allows for a finite Rashba SOC. In the host s-wave superconductor, it combines with the local magnetic-exchange fields to produce spin-triplet, odd-parity, $\pm p_x + ip_y$-wave pairing at the adatom sites [39]. Conversely, the exchange field at the adatom sites suppresses the s-wave order parameter. Therefore the adatom sites possess an admixture of spin-singlet s-wave and spin-triplet $\pm p_x + ip_y$-wave pairing. The spin-triplet correlations decay rapidly away from the adatom sites. An effective Josephson junction is, thus, formed in the vicinity of the adatom chain. A junction between a singlet and a triplet superconductor is predicted to accumulate spin because of the lifted spin-degeneracy of Andreev bound states (ABS) [40]. Concomitantly, Rashba SOC generates a persistent current, carried by the YSR states, around the magnetic impurities; the currents flow orthogonal to the local spin polarization [41].

Here, we show that the two different mechanisms, viz. the singlet-triplet Josephson junction and Rashba SOC, jointly cooperate to reinforce spin accumulation and spontaneous current flow around the adatom chains. Due to Rashba SOC, the accumulated spin provides an additional source for a circulating current around the adatom chain. The accumulated spins are polarized perpendicular to the direction of current flow and parallel to the local **d** vector of the triplet pairing amplitude. The s-wave pairing gap at the adatom site acquires a sign change as the YSR states undergo a parity-changing phase transition when the exchange coupling is tuned beyond a critical strength. The directions of both the spin polarization and the current are reversed at the same exchange-coupling strength at which Δ_s changes sign. The current is significantly enhanced in the topological superconducting regime and, therefore, can be used as an alternative probe for the identification of TSC and the experimental verification of MBS.

II. MODEL AND METHOD

We describe the adatom chain coupled to the host superconductor by the Hamiltonian $H_{\rm host} + H_{\rm imp}$. For a square lattice, $H_{\rm host}$ is written as

$$\begin{aligned} H_{\rm host} = &-t \sum_{\langle ij\rangle,\sigma} c^\dagger_{i\sigma} c_{j\sigma} - \mu \sum_{i,\sigma} c^\dagger_{i\sigma} c_{i\sigma} \\ &- i\alpha \sum_{\langle ij\rangle,\sigma,\sigma'} (\boldsymbol{\sigma} \times \mathbf{d}_{ij})^z_{\sigma\sigma'} c^\dagger_{i\sigma} c_{j\sigma'} \\ &+ \sum_i \left(\Delta^i_s c^\dagger_{i\uparrow} c^\dagger_{i\downarrow} + \Delta^{i*}_s c_{i\downarrow} c_{i\uparrow}\right), \end{aligned} \tag{1}$$

where t is the nearest-neighbor hopping amplitude of electrons, μ is the chemical potential, and α the strength of Rashba SOC;

$\mathbf{d}_{ij}$ denotes the unit vector between sites i and j. Below, all energy units will be measured in units of t. Furthermore, $\Delta_s^i = -U_s\langle c_{i\uparrow}c_{i\downarrow}\rangle$ is the local s-wave pairing gap, with the strength U_s of the onsite attraction. The adatom Hamiltonian $H_{\rm imp}$ is expressed as

$$H_{\rm imp} = -J\sum_{i\in\mathbf{I},\sigma,\sigma'}(\mathbf{S}_i\cdot\boldsymbol{\sigma}^z)_{\sigma\sigma'}c^\dagger_{i\sigma}c_{i\sigma'}, \qquad (2)$$

where J is the strength of the exchange coupling between the adatom spin $\mathbf{S}_i$ and the conduction-electron spin, and $\mathbf{I}$ denotes the sub-lattice corresponding to the adatom-chain sites. We assume that all the adatom spins are identical and ferromagnetically aligned along the z direction, which is perpendicular to the surface of the superconductor, i.e., $\mathbf{S}_i = S\hat{z}$.

With this choice of the Hamiltonian, the local pairing amplitudes and other site-resolved observables are determined using the self-consistent Bogoliubov-de Gennes (BdG) formalism [see Appendix]. To study the induced triplet-pairing amplitude on and near the chain, we add an equal-spin, nearest-neighbor, triplet term $H_{\rm triplet} = \sum_{\langle ij\rangle,\sigma}(\Delta^{t,ij}_{\sigma\sigma}c^\dagger_{i\sigma}c^\dagger_{j\sigma} + \Delta^{t,ij*}_{\sigma\sigma}c_{j\sigma}c_{i\sigma})$ where $\Delta^{t,ij}_{\sigma\sigma} = -U_t\langle c_{i\sigma}c_{j\sigma}\rangle$. U_t is the strength of the attractive interaction in the triplet channel. Such an interaction is generated by parity fluctuations in the presence of Rashba SOC and ferromagnetic exchange fields [42].

The total Hamiltonian $H_{\rm host} + H_{\rm imp} + H_{\rm triplet}$ is diagonalized to obtain the pairing amplitudes Δ^i_s and $\Delta^{t,ij}_{\sigma\sigma}$ in the self-consistent BdG evaluation, performed on an $N\times N$ square lattice with an adatom chain of length $N_{\rm imp}$ and open boundary conditions. Here, we show results for $U_t = U_s$, but we checked that the results, presented here, do not differ qualitatively for smaller values of U_t, even in the limit $U_t \to 0$. Here, we consider odd-parity triplet pairing amplitudes in the equal-spin pairing channels only, because the opposite-spin pairing states are suppressed in the absence of time-reversal symmetry (TRS) [43].

III. QUANTUM PHASE TRANSITIONS AND EMERGENCE OF TOPOLOGICAL SUPERCONDUCTIVITY

The pair of YSR states, originating from a single magnetic impurity in an s-wave superconductor, emerge from the continuum of bulk states and move symmetrically closer in energy within the bulk superconducting gap, as the impurity moment JS is increased. The total spin of the ground state changes when the pair of YSR states crosses zero energy at a critical value J_cS ($=1/\pi N_0$, where N_0 is the normal-state density of states at the Fermi level [44]). Beyond J_cS, the YSR states move apart and approach the bulk continuum states. For an adatom chain, the YSR states form a band and, there is a range $J_{c1}S \leqslant JS \leqslant J_{c2}S$ within which the YSR states remain close to zero energy. With a finite Rashba SOC and the inclusion of triplet pairing in the self-consistent calculation, there is a discontinuous change in energy of the YSR states for a single impurity at $J_cS = 2.56$ rather than a smooth crossover, and for an adatom chain, "zero-energy" MBS appear within the same range $J_{c1}S \leqslant JS \leqslant J_{c2}S$ (where $J_{c1}S = 2$ and $J_{c2}S = 3.9$), as shown in Fig. 1(a). The critical numbers J_cS, $J_{c1}S$, and $J_{c2}S$ depend on the strength of SOC [45]. To verify the MBS

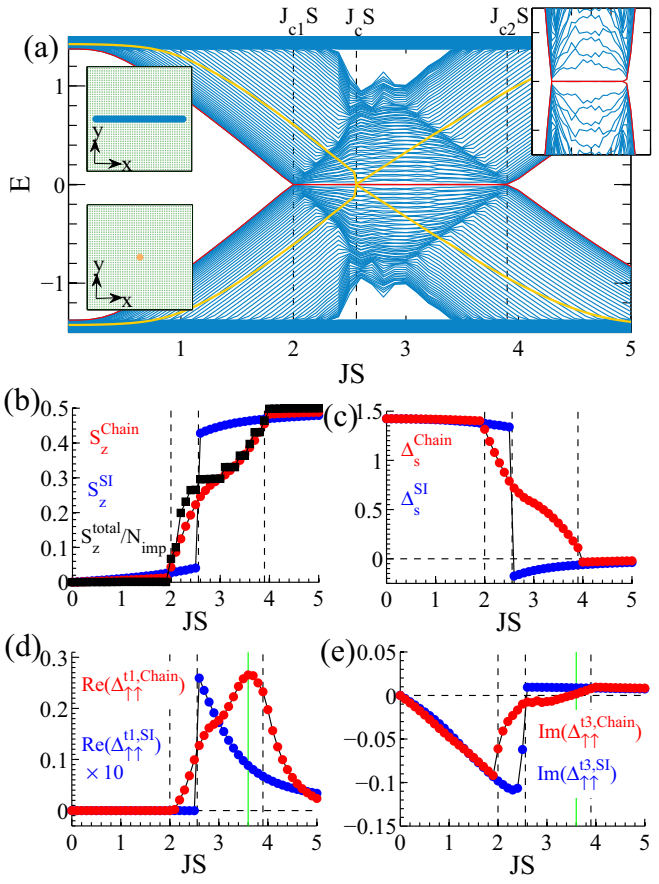

FIG. 1. (a) Variation of the BdG spectrum with impurity moment JS for a chain of length $N_{\rm imp} = 50$, on a superconducting square lattice of size 61×61. The yellow lines are the pair of YSR states for a single magnetic impurity in the same superconducting host. The insets on the left show the adatom configurations. The pair of red lines at zero energy represents the MBS within the range $J_{c1}S \leqslant JS \leqslant J_{c2}S$. (Right inset) Expanded view of the spectrum for the chain within the topological range. (b), (c), (d), and (e) show, respectively, the z component of spin-expectation value S_z, singlet pairing gap Δ_s, and triplet pairing amplitudes $\Delta^{t1}_{\uparrow\uparrow}$, $\Delta^{t3}_{\uparrow\uparrow}$, averaged along the chain, at the adatom sites or bonds with varying JS for a chain and a single impurity. The black square symbols in (b) show the total S_z, divided by $N_{\rm imp} = 15$, for a 21×21 lattice. The vertical green lines in (d) and (e) denote the value of JS at which $\mathrm{Re}(\Delta^{t1,\mathrm{Chain}}_{\uparrow\uparrow})$ is maximum and $\mathrm{Im}(\Delta^{t3,\mathrm{Chain}}_{\uparrow\uparrow})$ changes sign. Parameters taken: $t = 1$, $\mu = 0$, $\alpha = 0.1$, and $U_s = 3 = U_t$.

appearing within this range of JS, we plot the LDOS profile corresponding to the lowest pair of energy eigenvalues for a square lattice of size 61×61 with a 50-sites long adatom chain for $JS = 1$ (nontopological phase) in Fig. 2(a) and for $JS = 3$ (topological phase) in Fig. 2(b) For $JS = 1$, the LDOS profile is centered in the middle of the chain indicating that the YSR states are extended within the impurity chain. Instead, for $JS = 3$, the lowest-energy pair ($\pm2.8\times10^{-4}$) comes close to zero and the LDOS is concentrated at the two ends of the adatom chain. These sharp features at the chain-ends are the signatures of localized MBS. The pair of the zero-energy MBS is separated by a small energy gap, referred to as the

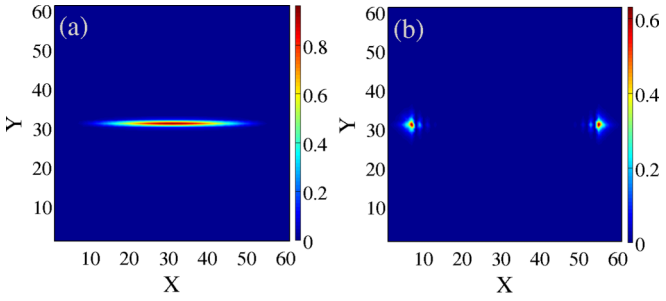

FIG. 2. The LDOS profile of an adatom chain of length $N_{\rm imp} = 50$, on a superconducting square lattice of size 61×61, corresponding to the pair of lowest energy eigenvalues for exchange-coupling strength (a) $JS = 1$ (nontopological phase), and $JS = 3$ (topological phase). The sharp peaks at the ends of the chain in (b) represent the zero-energy localized MBS. Parameters are the same as in Fig. 1.

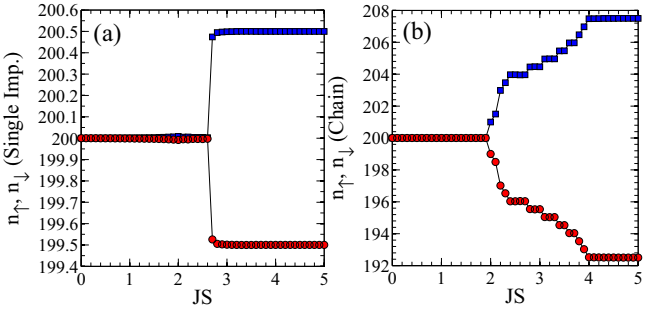

FIG. 3. Total number of up- and down-spin electrons, $n_\uparrow$ (blue) and $n_\downarrow$ (red), vs exchange coupling JS in the grand canonical ground state for (a) a single impurity and (b) an adatom chain. Calculations were performed on a 21×21 lattice. Parameters are the same as in Fig. 1.

minigap [46], from the YSR band states as shown in the inset of Fig. 1(a). The spatial extent of the MBS, centered at the two ends, decays exponentially with distance, but still gives rise to a finite overlap at the center of the chain, creating a tiny hybridization gap ($\sim10^{-4}$ for $N_{\rm imp} = 50$), which reduces with increasing chain length.

For a single magnetic impurity, the zero-energy level-crossing of the YSR states leads to a quantum phase transition as a localized quasiparticle excitation, with spin opposite to the impurity spin, is spontaneously created, forming an antiferromagnetic bound state with the impurity spin for $J < 0$ [39,44,47,48]. The transition at J_cS changes the total S_z of the ground state of the pairing Hamiltonian from $S_z = 0$ to $\pm1/2$, depending on the sign of J. On the other hand, the s-wave pairing amplitude Δ_s at the impurity site sharply drops in magnitude at J_cS and even encounters a sign change with respect to the bulk [44,49].

For an adatom chain, the transition in the total S_z of the conduction electrons $S_z = 1/2\sum_{i,\sigma,\sigma'}\langle c^\dagger_{i\sigma}\sigma^z_{\sigma\sigma'}c_{i\sigma'}\rangle$ and in the singlet pairing gap Δ_s take place within the same range $J_{c1}S \leqslant JS \leqslant J_{c2}S$ as depicted in Figs. 1(b) and 1(c). With increasing JS, the total S_z increases in discrete steps of height $1/2$ [50]. The sign change in Δ_s occurs at $J_{c2}S$ when $S_z = \frac{1}{2}N_{\rm imp}$. Also at $J_{c2}S$, the system becomes nontopological.

With increasing impurity moment JS, the total S_z of the superconductor, for a single impurity, increases by $\pm1/2$ (depending on the sign of J) at J_c. For an adatom chain, the total S_z increases in steps of height $1/2$ within the range $J_{c1}S \leqslant JS \leqslant J_{c2}S$ to the final value $\pm\frac{1}{2}N_{\rm imp}$. This increase corresponds to the spontaneous creation of quasiparticle excitations. However, the quasiparticle excitations in BdG evaluation of the pairing Hamiltonian always come in pairs. This is reflected in Fig. 3, which displays the total number of up- and down-spin electrons versus exchange coupling JS in the grand canonical ground state.

IV. INDUCED TRIPLET PAIRING

We calculate the triplet pairing amplitudes $\Delta^{t,ij}_{\sigma\sigma}$ on the four bonds connected to the chain site i viz. $\Delta^{t1}_{\sigma\sigma} = \Delta^{i,i+\hat{x}}_{\sigma\sigma}$, $\Delta^{t2}_{\sigma\sigma} = \Delta^{i,i-\hat{x}}_{\sigma\sigma}$, $\Delta^{t3}_{\sigma\sigma} = \Delta^{i,i+\hat{y}}_{\sigma\sigma}$, and $\Delta^{t4}_{\sigma\sigma} = \Delta^{i,i-\hat{y}}_{\sigma\sigma}$. Due to the inherent p-wave symmetry, we obtain: $\Delta^{t2}_{\sigma\sigma} = -\Delta^{t1}_{\sigma\sigma}$ and $\Delta^{t4}_{\sigma\sigma} = -\Delta^{t3}_{\sigma\sigma}$. Furthermore, we find $\mathrm{Im}(\Delta^{t1}_{\sigma\sigma}) = \mathrm{Re}(\Delta^{t3}_{\sigma\sigma}) = 0$, $\mathrm{Re}(\Delta^{t1}_{\uparrow\uparrow}) = -\mathrm{Re}(\Delta^{t1}_{\downarrow\downarrow})$ and $\mathrm{Im}(\Delta^{t3}_{\uparrow\uparrow}) = \mathrm{Im}(\Delta^{t3}_{\downarrow\downarrow})$. This implies $-p_x + ip_y$-wave pairing for the $\uparrow\uparrow$ channel and $p_x + ip_y$-wave pairing for the $\downarrow\downarrow$ channel. Figures 1(d) and 1(e) show the variation of the triplet pairing amplitudes with JS. For a single impurity, these amplitudes reveal sharp jumps at J_cS, along with a sign change in $\mathrm{Im}(\Delta^{t3}_{\sigma\sigma})$. For the adatom chain, the transition proceeds within the range $J_{c1}S \leqslant JS \leqslant J_{c2}S$, along with a maximum in $\mathrm{Re}(\Delta^{t1}_{\sigma\sigma})$ and a sign change in $\mathrm{Im}(\Delta^{t3}_{\sigma\sigma})$ at $J_{cs}S = 3.6$ [denoted by a green vertical line in Figs. 1(d)–1(e)]. Hence, at $J_{cs}S$, there is a change in pairing symmetry from $\pm p_x + ip_y$ wave to $\pm p_x - ip_y$ wave ($\pm$ refers to pairing in $\uparrow\uparrow$ and $\downarrow\downarrow$ channels, respectively). The triplet pairing amplitudes reflect the broken TRS at the adatom sites.

To study the spatial confinement of the induced triplet pairing amplitude, we plot in Fig. 4 the profile of the magnetization, the singlet and triplet pairing amplitudes in the two-dimensional lattice plane.

We find that the induced triplet pairing is confined to the vicinity of the adatom chain and die off quickly at sites further away from the chain. The s-wave pairing gap Δ_s is significantly suppressed because of the local magnetization along the chain, as shown in Figs. 4(a) and 4(b). Interestingly, the triplet order parameters $\mathrm{Re}(\Delta^{t,1}_{\uparrow\uparrow})$ and $\mathrm{Im}(\Delta^{t,3}_{\uparrow\uparrow})$ reveal maximum amplitudes at the ends of the chain only in the topological superconducting regime, as shown in Figs. 4(c) and 4(d). It was, in fact, proposed that MBS on the boundary of topological superconductors have universal spin-triplet correlations [51]. There is a sign change in $\mathrm{Re}(\Delta^{t,1}_{\uparrow\uparrow})$ at the two ends of the chain indicating the realization of chiral p-wave triplet pairing. The results demonstrate that a mixed singlet-triplet pairing is realized in the chain and, thus an effective Josephson junction is formed in the vicinity of the chain. The consequences of the Josephson junction is discussed in Sec. V.

For a conventional BCS superconductor, the superconducting critical temperature T_c and the pairing amplitude Δ are related to the attractive interaction strength U via $k_BT_c = 1.13\,E_D\,e^{-1/N(0)U}$ and $\Delta(T=0) = 1.76\,k_BT_c$, where E_D is a cutoff energy for pairing and $N(0)$ is the density of states at the Fermi level. In order to check the nature of the induced triplet pairing in the adatom chain, we plot the logarithm of the triplet pairing amplitude $\Delta_t = \mathrm{Re}(\Delta^{t1}_{\uparrow\uparrow})$ with U_t in Fig. 5.

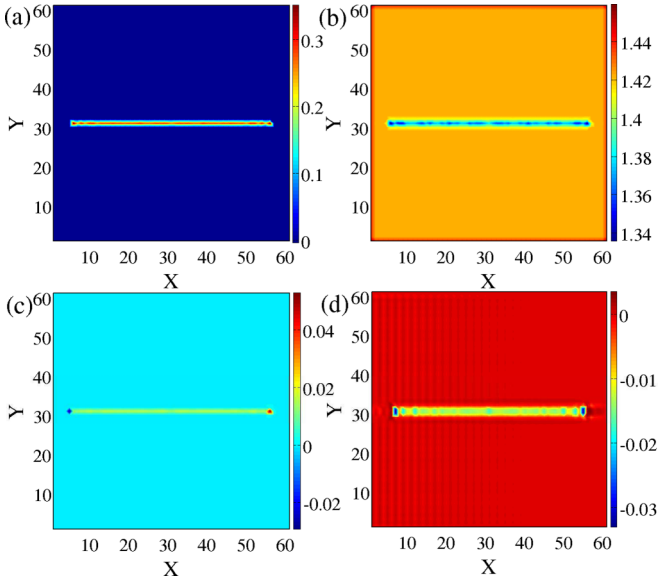

FIG. 4. The spatial profile of (a) z component of spin-expectation value S_z, (b) singlet s-wave superconducting order parameter Δ_s, (c) real part of triplet pairing gap for the bond along $+x$ direction, $\mathrm{Re}(\Delta^{t,1}_{\uparrow\uparrow})$, and (d) imaginary part of triplet pairing gap for the bond along $+y$ direction, $\mathrm{Im}(\Delta^{t,3}_{\uparrow\uparrow})$, calculated for $JS = 3$ (topological superconducting phase). A square lattice of size 61×61 was used for the calculation with impurity-chain length $N_{\mathrm{imp}} = 50$ and parameters of Fig. 1.

In the $U_t \to 0$ limit, $\ln(\Delta_t)$ approaches a finite, small number. The results establish that the induced triplet pairing on the adatom chain is of conventional weak coupling character.

V. SPONTANEOUS SPIN ACCUMULATION AND FLOW OF PERSISTENT CURRENT

The triplet pairing is confined to the near vicinity of the adatom chain, and, therefore, an effective Josephson junction is formed between the chain region with pairing symmetry $s \pm p_x + ip_y$ and the surrounding host superconductor with s-wave symmetry. The resultant spin profile near the chain is

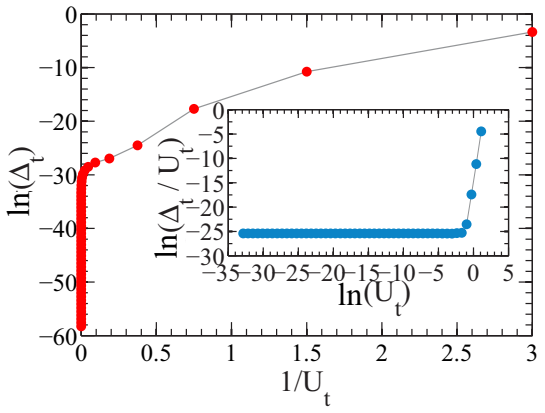

FIG. 5. Variation of the triplet order parameter Δ_t in natural logarithmic scale with the attractive interaction strength U_t for impurity moment $JS = 3$. Inset shows the variation of $\ln(\Delta_t/U_t)$ with $\ln(U_t)$. Other parameters are the same as in Fig. 4.

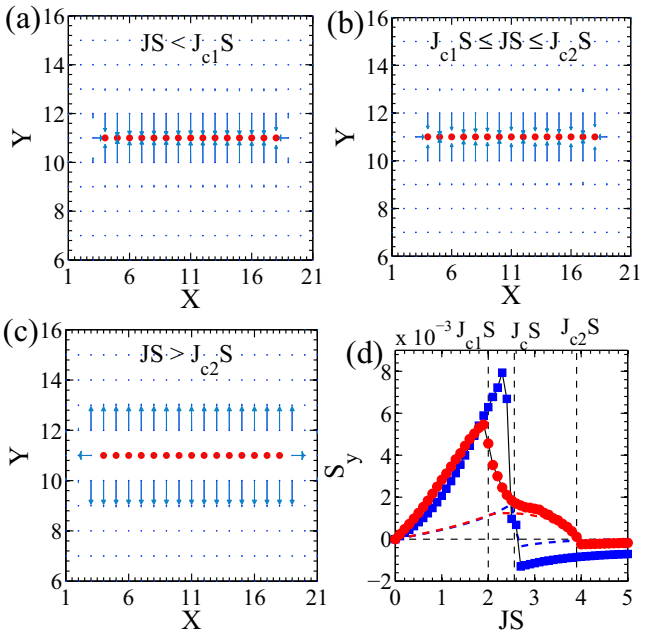

FIG. 6. Profile of the accumulated spins near the adatom chain for (a) $JS = 1(<J_{c1}S)$, (b) $JS = 3(J_{c1}S \leqslant JS \leqslant J_{c2}S)$, and (c) $JS = 5(>J_{c2}S)$, calculated on a 21×21 lattice with $N_{\mathrm{imp}} = 15$. The red symbols mark the adatom sites. The length of the arrows is amplified for visualization purpose. (d) Variation of the spin-expectation value S_y, averaged over the sites just below the chain, with impurity moment JS for finite U_t and $U_t = 0$ (solid symbols and dashed lines, respectively) in case of a single magnetic impurity (blue) and a chain (red). Parameters are the same as in Fig. 1.

plotted in Figs. 6(a)–6(c), in the three regimes, i.e., $JS < J_{c1}S$, $J_{c1}S \leqslant JS \leqslant J_{c2}S$, and $JS > J_{c2}S$. The spins near the chain point towards and away from the chain, respectively, for JS below and above $J_{c2}S$.

Enhancing the triplet-pairing amplitude at the junction also increases the magnitude of the accumulated spins which are polarized in the direction of the local $\mathbf{d}$ vector (in Balian-Werthamer representation) of the triplet pairing amplitude [40,52]. To identify the connection between the polarization of the accumulated spins near the chain and the induced triplet pairing, we plot the local $\mathbf{d}$ vector of the triplet pairing amplitude in real space in Fig. 7. In Balian-Werthamer representation, the pairing matrix can be written as

$$\begin{pmatrix} \Delta_{\uparrow\uparrow} & \Delta_{\uparrow\downarrow} \\ \Delta_{\downarrow\uparrow} & \Delta_{\downarrow\downarrow} \end{pmatrix} = (\Delta_s + \boldsymbol{\sigma}\cdot\mathbf{d})i\sigma_2 = \begin{pmatrix} -d_x + id_y & \Delta_s + d_z \\ -\Delta_s + d_z & d_x + id_y \end{pmatrix}. \quad (3)$$

We verified that the d_z component has a tiny value because of broken TRS [43]. The other two components are calculated via $d_x = -(\Delta_{\uparrow\uparrow} - \Delta_{\downarrow\downarrow})/2$ and $d_y = \mathrm{Im}(\Delta_{\uparrow\uparrow} + \Delta_{\downarrow\downarrow})/2$. It is evident that the $\mathbf{d}$ vector flips its direction beyond $J_{cs}S$, as also found from Fig. 1(e). The reorientation of the $\mathbf{d}$ vector and the sign change in Δ_s both occur at the same critical impurity moment J_cS for a single magnetic impurity. However, for an

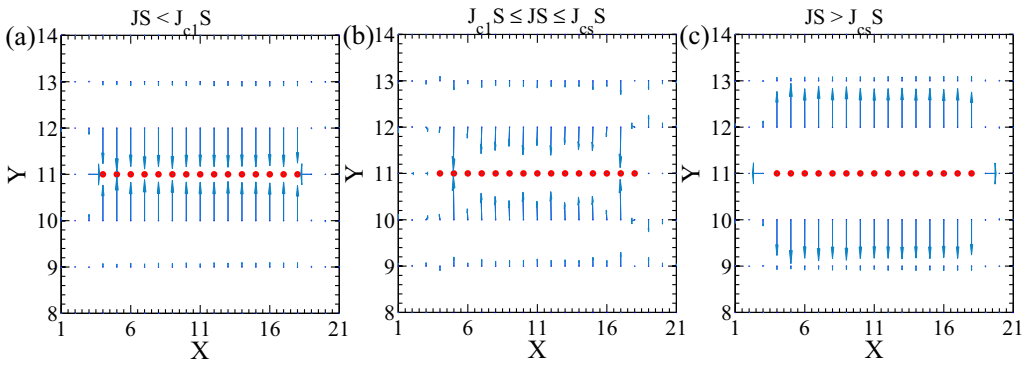

FIG. 7. The real-space profile of the local **d**-vector of the triplet pairing amplitude for (a) $JS = 1$ (trivial phase), (b) $JS = 3$ (topological superconducting phase), and (c) $JS = 5$ (trivial phase). Other parameters are the same as in Fig. 4.

adatom chain, the **d** vector flips its direction at $J_{cs}S$ while Δ_s changes sign at $J_{c2}S$.

To get quantitative information about the spin polarization and the value of JS at which the spins flip their directions, we calculate $S_y = 1/2\langle\sigma_y\rangle$ at the neighboring sites below the adatom chain, with $U_t = 0$ and with finite U_t, and plot the average value with increasing JS in Fig. 6(d). With finite U_t, S_y acquires significantly larger values below $J_{c1}S$ compared to that in the case of $U_t = 0$. The amplitude of S_y follows the behavior of $\mathrm{Im}(\Delta^{t3}_{\sigma\sigma})$, suggesting a close connection between the accumulated spin and the triplet pairing amplitude. S_y changes sign at J_cS for a single impurity and at $J_{c2}S$ for an adatom chain. The sign change in $\mathrm{Im}(\Delta^{t3}_{\sigma\sigma})$ at $J_{cs}S$ is not reflected in S_y owing to the small amplitude of $\mathrm{Im}(\Delta^{t3}_{\sigma\sigma})$ near

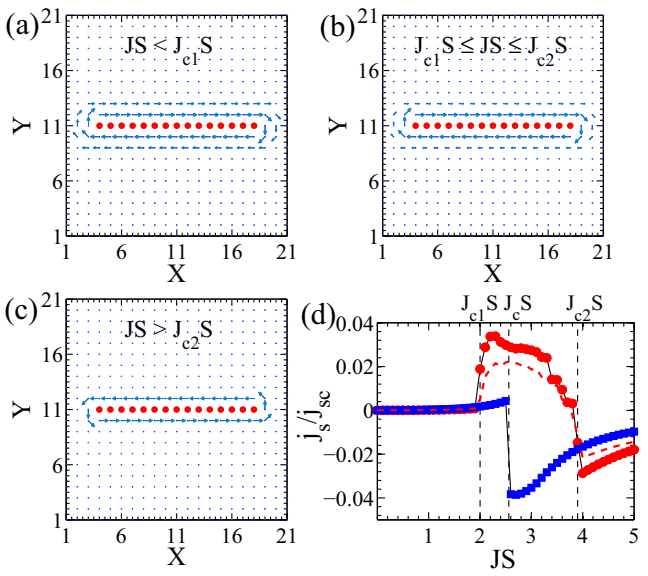

FIG. 8. Current flow around the adatom chain for (a) $JS = 1(<J_{c1}S)$, (b) $JS = 3(J_{c1}S \leqslant JS \leqslant J_{c2}S)$, and (c) $JS = 5(>J_{c2}S)$, calculated on a 21×21 lattice with $N_{\mathrm{imp}} = 15$. The red symbols mark the adatom sites. (d) Variation of the magnitude of the current $\mathbf{j_s}$, normalized by the critical supercurrent for the host superconductor $\mathbf{j_{sc}}$, with the impurity moment JS for a single magnetic impurity (blue squares) and an adatom chain (red circles). The dashed line shows the variation of the current with JS for $U_t = 0$. Parameters are the same as in Fig. 1.

J_{cs}. The exchange coupling jointly with Rashba SOC control the sign change in S_y at $J_{c2}S$ when Δ_s also changes sign.

Rashba SOC gives rise to an additional contribution to the paramagnetic current operator, the expectation value of which depends upon the magnetization profile. A magnetic impurity or a ferromagnetic island, proximity coupled to a superconductor, renders a finite spin polarization around the impurity or the island, giving rise to a SOC-driven current [41,53]. Hence the spin accumulation near the chain generates a current in the superconductor which circulates around the chain. Driving a current via magnetism is referred to as the magnetoelectric effect [54]. The contribution to the current operator $\mathbf{j}_s^{\mathrm{SOC}} = (j_{sx}, j_{sy})$ originating from Rashba SOC is given by

$$j_{sx/sy} = \mp\alpha\frac{e}{\hbar}\sum_{\sigma,\sigma'}(\sigma_{y/x})_{\sigma\sigma'}(c^{\dagger}_{i+\hat{x}/\hat{y},\sigma}c_{i,\sigma'} - c^{\dagger}_{i,\sigma'}c_{i+\hat{x}/\hat{y},\sigma}),$$

following the Peierls-factor derivation of Ref. [55]. The rising of $S_{x/y}$ at sites next to the adatom chain, induced by the singlet-triplet junction, leads to an enhanced current around the chain as described in Fig. 8. For a single magnetic impurity, the current $\mathbf{j}_s$ drops to a large negative value and changes its sense of circulation at J_cS where Δ_s changes sign. However, for an adatom chain, $\mathbf{j}_s$ rises to higher values at $J_{c1}S$ (a few percent of the critical current $\mathbf{j}_{sc} = 2e\Delta/\pi\hbar$ for the host superconductor [56]), decreases nonmonotonically and finally reverses its propagation direction at $J_{c2}S$ as shown in Figs. 8(a)–8(a). The nonmonotonic behavior of $\mathbf{j}_s$ between $J_{c1}S$ and $J_{c2}S$, including the steps, may be envisaged as a conjugate effect of (i) decrease in S_y of the accumulated spins and (ii) the stepwise increase in total S_z of the superconductor. When the ferromagnetic adatoms point towards the in-plane direction instead of the out-of-plane direction, the current pattern changes qualitatively. In this case, the current vectors loose the circulation pattern around the adatom chain and point predominantly perpendicular to the adatom spins [41]. The amplitude of the current, however, exhibits similar enhancement within two specific values of JS.

VI. DISCUSSION

The magnetic-adatom chains have certainly received particular attention because of the existence of MBS at the

chain ends. However, as our results demonstrate, the physics of the adatom chains contains far more intriguing aspects, which originate from Rashba SOC. The accumulated spin polarization and the spin-triplet pairing amplitudes can possibly be detected by local spin-resolved probes with STM techniques [57], while the orbital magnetic moment of the persistent current around the adatom chains should be measurable using scanning SQUID sensors. The existence of the MBS, as inferred from STM experiments, appears still ambiguous primarily because of experimental challenges in disentangling the MBS from the YSR states near zero energy [58]. The simultaneous detection of the circulating currents would therefore provide a further piece of evidence in support of topological superconductivity and the interpretation of the STM signals in favor of MBS.

Regarding the experimental detectability of the enhanced persistent currents, we can perform the following estimates: we start from the critical current density of Pb, which is $j_c = 10^6$ A/cm^2. If this current flows in the top two surface layers, the lattice constant of Pb, $a = 5\times10^{-8}$ cm, allows to translate this critical current density into the current $I_c = j_c a^2 = 2.5\times10^{-9}$ A. Our calculations gave a maximum persistent current of $I = 0.05 I_c = 1.25\times10^{-10}$ A. For a chain of 15 adatoms, this current encircles an area of $30\,a^2$, which leads to a magnetic moment of $10^{-4}\mu_B$. On the other hand, for a circular current flow around the same area the magnetic field strength at the center of the circular loop reaches 5×10^{-8} T. If a scanning SQUID is placed at a typical minimum distance of 100 nm above the current loop, the magnetic field is still of the order 2×10^{-13} T and therefore within the range of detectability.

For a particular choice of adatoms (Fe or Co) and their configuration on the surface, the parameters J and S are fixed and it is not possible to explore different phases in one experiment. The issue could be circumvented by applying a homogeneous magnetic field to rotate the spin polarization of the adatoms. In the current analysis, we assumed the adatom spins to point towards the z direction, i.e., perpendicular to the surface of the superconductor. Since Rashba SOC breaks the spin SU(2) symmetry, the YSR states depend on the polar angle θ of the adatom spins and a topological phase transition can be induced by tuning θ [45,59]. A magnetic-field rotation experiment may thereby tune to the topological regime using the circulating current as a probe. The phenomena, identified here, are equally applicable to islands of adatoms where MBS convert to edge-bound modes.

ACKNOWLEDGMENTS

The authors acknowledge discussions with Dirk Morr, Stephan Rachel, and Titus Neupert. This work was supported by the Deutsche Forschungsgemeinschaft through TRR 80. Computations were performed at the Leibniz-Rechenzentrum in Munich.

APPENDIX: SELF-CONSISTENT BOGOLIUBOV-DE GENNES (BDG) FORMALISM

The total Hamiltonian $H_{\rm tot} = H_{\rm host} + H_{\rm imp} + H_{\rm triplet}$ for a spin-orbit coupled superconductor with an adatom chain is written in a square lattice as

$$\begin{aligned} H_{\rm tot} = &-t\sum_{\langle ij\rangle,\sigma} c^\dagger_{i\sigma}c_{j\sigma} - \mu\sum_{i,\sigma} c^\dagger_{i\sigma}c_{i\sigma} \\ &- J\sum_{i\in\mathbf{I},\sigma,\sigma'} (\mathbf{S}_i\cdot\boldsymbol{\sigma}^z)_{\sigma\sigma'}c^\dagger_{i\sigma}c_{i\sigma'} \\ &- i\alpha\sum_{\langle ij\rangle,\sigma,\sigma'} (\boldsymbol{\sigma}\times\mathbf{d}_{ij})^z_{\sigma\sigma'}c^\dagger_{i\sigma}c_{j\sigma'} \\ &+ \sum_i(\Delta_i c^\dagger_{i\uparrow}c^\dagger_{i\downarrow} + \Delta^*_i c_{i\downarrow}c_{i\uparrow}) \\ &+ \sum_{\langle ij\rangle,\sigma}\left(\Delta^{\sigma\sigma}_{ij}c^\dagger_{i\sigma}c^\dagger_{j\sigma} + \Delta^{\sigma\sigma*}_{ij}c_{j\sigma}c_{i\sigma}\right), \end{aligned} \tag{A1}$$

where t is the hopping amplitude, μ is the chemical potential, J is the exchange coupling strength of the adatom spin $\mathbf{S}_i$ (assumed to be polarized along the z direction) with the conduction electrons. $\mathbf{I}$ denotes the sublattice of the adatom chain, α is the strength of Rashba spin-orbit coupling, and $\mathbf{d}_{ij}$ the unit vector between nearest-neighbor sites i and j. $\Delta_i = -U_s\langle c_{i\uparrow}c_{i\downarrow}\rangle$ is the on-site singlet pairing gap with the attractive pairing potential U_s and $\Delta^{\sigma\sigma}_{ij} = -U_t\langle c_{i\sigma}c_{j\sigma}\rangle$ denotes the nearest-neighbor equal-spin pairing gap with the attractive triplet pairing potential U_t.

The above Hamiltonian is diagonalized using the Bogoliubov-Valatin transformation:

$$c_{i\sigma} = \sum_{n,\sigma'}\left[u^i_{n\sigma\sigma'}\gamma_{n\sigma'} + v^{i*}_{n\sigma\sigma'}\gamma^\dagger_{n\sigma'}\right], \tag{A2}$$

where $\gamma^\dagger_{n\sigma'}$ ($\gamma_{n\sigma'}$) is a fermionic operator which describes the creation (destruction) of a BdG state with spin σ' in the nth eigenstate of $H_{\rm tot}$; $u^i_{n\sigma\sigma'}$ and $v^i_{n\sigma\sigma'}$ are the particle and hole amplitudes, respectively. After diagonalization, $H_{\rm tot}$ is rewritten in terms of $u^i_{n\sigma\sigma'}$ and $v^i_{n\sigma\sigma'}$. It is convenient, therefore, to remove the index σ' attached to these variables, whereby the summation over σ' is implicitly subjoined in the sum over n. The BdG equations can finally be written, in the matrix form, as

$$\begin{aligned} \sum_i &\begin{pmatrix} \Gamma^{\uparrow\uparrow}_{ij} & \Gamma^{\uparrow\downarrow}_{ij} & \Delta^{\uparrow\uparrow}_{ij} & \Delta^{\uparrow\downarrow}_{ij} \\ \Gamma^{\downarrow\uparrow}_{ij} & \Gamma^{\downarrow\downarrow}_{ij} & -\Delta^{\downarrow\uparrow}_{ij} & \Delta^{\downarrow\downarrow}_{ij} \\ \Delta^{\uparrow\uparrow*}_{ij} & -\Delta^{\downarrow\uparrow*}_{ij} & -\Gamma^{\uparrow\uparrow*}_{ij} & -\Gamma^{\uparrow\downarrow*}_{ij} \\ \Delta^{\uparrow\downarrow*}_{ij} & \Delta^{\downarrow\downarrow*}_{ij} & -\Gamma^{\downarrow\uparrow*}_{ij} & -\Gamma^{\downarrow\downarrow*}_{ij} \end{pmatrix}\begin{pmatrix} u^j_{n\uparrow} \\ u^j_{n\downarrow} \\ v^j_{n\uparrow} \\ v^j_{n\downarrow} \end{pmatrix} \\ &= E_n\begin{pmatrix} u^j_{n\uparrow} \\ u^j_{n\downarrow} \\ v^j_{n\uparrow} \\ v^j_{n\downarrow} \end{pmatrix}, \end{aligned} \tag{A3}$$

where $\Gamma^{\sigma\sigma'}_{ij} = -t(1-\delta_{ij})\delta_{\sigma\sigma'} - \mu\delta_{ij}\delta_{\sigma\sigma'} - J(\mathbf{S}_i\cdot\boldsymbol{\sigma}^z)_{\sigma\sigma'}\delta_{ij}(1-\delta_{\sigma\sigma'}) - i\alpha(\boldsymbol{\sigma}\times\mathbf{d}_{ij})^z_{\sigma\sigma'}(1-\delta_{ij})(1-\delta_{\sigma\sigma'})$ (δ's are the Kronecker's delta functions) and E_n is the energy of nth eigenstate. For a square lattice of size $N\times N$, the above matrix is of dimension $4N^2\times4N^2$.

The local pairing amplitudes and the magnetization components are written in terms of the particle and hole amplitudes

as

$$\begin{aligned}
\Delta_i &= -U_s\langle c_{i\uparrow}c_{i\downarrow}\rangle \\
&= -U_s\sum_n\left[u^i_{n\uparrow}v^{i*}_{n\downarrow}(1-f(E_n))+u^i_{n\downarrow}v^{i*}_{n\uparrow}f(E_n)\right], \\
\Delta^{\sigma\sigma}_{ij} &= -U_t\langle c_{i\sigma}c_{j\sigma}\rangle \\
&= -U_t\sum_n\left[u^i_{n\sigma}v^{j*}_{n\sigma}(1-f(E_n))+u^i_{n\sigma}v^{j*}_{n\sigma}f(E_n)\right], \\
S_{xi} &= \frac{1}{2}\langle c^\dagger_{i\uparrow}c_{i\downarrow}+c^\dagger_{i\downarrow}c_{i\uparrow}\rangle \\
&= \frac{1}{2}\sum_n\left[\left(u^{i*}_{n\uparrow}u^i_{n\downarrow}+u^{i*}_{n\downarrow}u^i_{n\uparrow}\right)f(E_n)\right. \\
&\quad\left.+\left(v^i_{n\uparrow}v^{i*}_{n\downarrow}+v^i_{n\downarrow}v^{i*}_{n\uparrow}\right)(1-f(E_n))\right], \\
S_{yi} &= \frac{-i}{2}\langle c^\dagger_{i\uparrow}c_{i\downarrow}-c^\dagger_{i\downarrow}c_{i\uparrow}\rangle \\
&= \frac{1}{2}\sum_n\left[(u^{i*}_{n\uparrow}u^i_{n\downarrow}-u^{i*}_{n\downarrow}u^i_{n\uparrow})f(E_n)\right. \\
&\quad\left.+\left(v^i_{n\uparrow}v^{i*}_{n\downarrow}-v^i_{n\downarrow}v^{i*}_{n\uparrow}\right)(1-f(E_n))\right], \\
S_{zi} &= \frac{1}{2}\langle c^\dagger_{i\uparrow}c_{i\uparrow}-c^\dagger_{i\downarrow}c_{i\downarrow}\rangle \\
&= \frac{1}{2}\sum_n\left[\left(\left|u^{i*}_{n\uparrow}\right|^2-\left|u^{i*}_{n\downarrow}\right|^2\right)f(E_n)\right. \\
&\quad\left.+\left(\left|v^{i*}_{n\uparrow}\right|^2-\left|v^{i*}_{n\downarrow}\right|^2\right)(1-f(E_n))\right], \qquad \text{(A4)}
\end{aligned}$$

where $f(E_n)$ is the Fermi-Dirac distribution function, entering in the above equations via the relations: $\langle\gamma^\dagger_n\gamma_n\rangle = f(E_n)$ and $\langle\gamma_n\gamma^\dagger_n\rangle = 1-f(E_n)$. In what follows, iterations are performed using Eqs. (A3) and (A4) until self-consistency is achieved at every sites, and finally the local order parameters are computed using Eqs. (A4).

The local density of states (LDOS) is given by

$$\rho_i(E) = \frac{1}{N^2}\sum_{n,\sigma}\left[\left|u^i_{n\sigma}\right|^2\delta(E-E_n)+\left|v^i_{n\sigma}\right|^2\delta(E+E_n)\right], \qquad \text{(A5)}$$

where $\delta(E\pm E_n)$ are the Dirac delta functions which are approximated by Gaussian functions in the numerical evaluations.

[1] S. Nadj-Perge, I. K. Drozdov, B. A. Bernevig, and A. Yazdani, Phys. Rev. B **88**, 020407 (2013).
[2] J. Li, T. Neupert, Z. Wang, A. H. MacDonald, A. Yazdani, and B. A. Bernevig, Nat. Commun. **7**, 12297 (2016).
[3] J. Röntynen and T. Ojanen, Phys. Rev. Lett. **114**, 236803 (2015).
[4] S. Nadj-Perge, I. K. Drozdov, J. Li, H. Chen, S. Jeon, J. Seo, A. H. MacDonald, B. A. Bernevig, and A. Yazdani, Science **346**, 602 (2014).
[5] B. E. Feldman, M. T. Randeria, J. Li, S. Jeon, Y. Xie, Z. Wang, I. K. Drozdov, B. A. Bernevig, and A. Yazdani, Nat. Phys. **13**, 286 (2017).
[6] R. Pawlak, M. Kisiel, J. Klinovaja, T. Meier, S. Kawai, T. Glatzel, D. Loss, and E. Meyer, npj Quantum Inf. **2**, 16035 (2016).
[7] M. Ruby, F. Pientka, Y. Peng, F. von Oppen, B. W. Heinrich, and K. J. Franke, Phys. Rev. Lett. **115**, 197204 (2015).
[8] M. Ruby, B. W. Heinrich, Y. Peng, F. von Oppen, and K. J. Franke, Nano Lett. **17**, 4473 (2017).
[9] G. C. Ménard, S. Guissart, C. Brun, M. Trif, F. Debontridder, R. T. Leriche, D. Demaille, D. Roditchev, P. Simon, and T. Cren, Nat. Commun. **8**, 2040 (2017).
[10] L. Fu and C. L. Kane, Phys. Rev. Lett. **100**, 096407 (2008).
[11] R. M. Lutchyn, J. D. Sau, and S. Das Sarma, Phys. Rev. Lett. **105**, 077001 (2010).
[12] V. Mourik, K. Zuo, S. M. Frolov, S. R. Plissard, E. P. A. M. Bakkers, and L. P. Kouwenhoven, Science **336**, 1003 (2012).
[13] N. Mohanta and A. Taraphder, Europhys. Lett. **108**, 60001 (2014).
[14] I. Reis, D. J. J. Marchand, and M. Franz, Phys. Rev. B **90**, 085124 (2014).
[15] P. M. R. Brydon, S. Das Sarma, H.-Y. Hui, and J. D. Sau, Phys. Rev. B **91**, 064505 (2015).
[16] M. H. Christensen, M. Schecter, K. Flensberg, B. M. Andersen, and J. Paaske, Phys. Rev. B **94**, 144509 (2016).
[17] Y. Luh, Acta Phys. Sin. **21**, 75 (1965).
[18] H. Shiba, Prog. Theor. Phys. **40**, 435 (1968).
[19] A. I. Rusinov, Sov. Phys.–JETP **29**, 1101 (1969).
[20] A. Heimes, D. Mendler, and P. Kotetes, New J. Phys. **17**, 023051 (2015).
[21] K. Pöyhönen, A. Westström, and T. Ojanen, Phys. Rev. B **93**, 014517 (2016).
[22] F. Pientka, L. I. Glazman, and F. von Oppen, Phys. Rev. B **88**, 155420 (2013).
[23] Y. Peng, F. Pientka, L. I. Glazman, and F. von Oppen, Phys. Rev. Lett. **114**, 106801 (2015).
[24] J. Li, H. Chen, I. K. Drozdov, A. Yazdani, B. A. Bernevig, and A. H. MacDonald, Phys. Rev. B **90**, 235433 (2014).
[25] T. Neupert, A. Yazdani, and B. A. Bernevig, Phys. Rev. B **93**, 094508 (2016).
[26] K. Björnson and A. M. Black-Schaffer, Phys. Rev. B **94**, 100501 (2016).
[27] T. Cadez and P. D. Sacramento, J. Phys.: Condens. Matter **28**, 495703 (2016).
[28] J. Zhang and V. Aji, Phys. Rev. B **94**, 060501 (2016).
[29] J. Zhang, Y. Kim, E. Rossi, and R. M. Lutchyn, Phys. Rev. B **93**, 024507 (2016).
[30] A. Westström, K. Pöyhönen, and T. Ojanen, Phys. Rev. B **91**, 064502 (2015).
[31] J. Röntynen and T. Ojanen, Phys. Rev. B **90**, 180503 (2014).
[32] A. Heimes, P. Kotetes, and G. Schön, Phys. Rev. B **90**, 060507 (2014).
[33] F. Pientka, L. I. Glazman, and F. von Oppen, Phys. Rev. B **89**, 180505 (2014).
[34] K. Pöyhönen, A. Westström, J. Röntynen, and T. Ojanen, Phys. Rev. B **89**, 115109 (2014).
[35] H.-Y. Hui, P. M. R. Brydon, J. D. Sau, S. Tewari, and S. D. Sarma, Sci. Rep. **5**, 8880 (2015).

[36] J. Klinovaja, P. Stano, A. Yazdani, and D. Loss, Phys. Rev. Lett. **111**, 186805 (2013).
[37] S. Hoffman, J. Klinovaja, and D. Loss, Phys. Rev. B **93**, 165418 (2016).
[38] A. Y. Kitaev, Phys. Usp. **44**, 131 (2001).
[39] S. Rachel, E. Mascot, S. Cocklin, M. Vojta, and D. K. Morr, Phys. Rev. B **96**, 205131 (2017).
[40] K. Sengupta and V. M. Yakovenko, Phys. Rev. Lett. **101**, 187003 (2008).
[41] S. S. Pershoguba, K. Björnson, A. M. Black-Schaffer, and A. V. Balatsky, Phys. Rev. Lett. **115**, 116602 (2015).
[42] V. Kozii and L. Fu, Phys. Rev. Lett. **115**, 207002 (2015).
[43] M. Sigrist, AIP Conf. Proc. **1162**, 55 (2009).
[44] A. V. Balatsky, I. Vekhter, and J.-X. Zhu, Rev. Mod. Phys. **78**, 373 (2006).
[45] Y. Kim, J. Zhang, E. Rossi, and R. M. Lutchyn, Phys. Rev. Lett. **114**, 236804 (2015).
[46] S. Tewari, T. D. Stanescu, J. D. Sau, and S. Das Sarma, Phys. Rev. B **86**, 024504 (2012).
[47] A. Sakurai, Prog. Theor. Phys. **44**, 1472 (1970).
[48] M. I. Salkola, A. V. Balatsky, and J. R. Schrieffer, Phys. Rev. B **55**, 12648 (1997).
[49] K. Björnson, A. V. Balatsky, and A. M. Black-Schaffer, Phys. Rev. B **95**, 104521 (2017).
[50] D. K. Morr and J. Yoon, Phys. Rev. B **73**, 224511 (2006).
[51] X. Liu, J. D. Sau, and S. Das Sarma, Phys. Rev. B **92**, 014513 (2015).
[52] C.-K. Lu and S. Yip, Phys. Rev. B **80**, 024504 (2009).
[53] K. Björnson, S. S. Pershoguba, A. V. Balatsky, and A. M. Black-Schaffer, Phys. Rev. B **92**, 214501 (2015).
[54] V. M. Edelstein, Phys. Rev. B **72**, 172501 (2005).
[55] D. J. Scalapino, S. R. White, and S. Zhang, Phys. Rev. B **47**, 7995 (1993).
[56] P. F. Bagwell, Phys. Rev. B **49**, 6841 (1994).
[57] M. Graham and D. K. Morr, Phys. Rev. B **96**, 184501 (2017).
[58] F. Pientka, Y. Peng, L. Glazman, and F. von Oppen, Phys. Scr. (2015) 014008.
[59] F. Loder, A. P. Kampf, and T. Kopp, Sci. Rep. **5**, 15302 (2015).